

## Article

# Explaining Color Change in Gem-Quality Andradite Garnet

Jia-Hong Xu <sup>1,2</sup>, Xiao-Yan Yu <sup>1,\*</sup>, Mei Shen <sup>3</sup>, Ying Yan <sup>1</sup> and Guang-Ya Wang <sup>1,2</sup>

<sup>1</sup> School of Gemology, China University of Geosciences Beijing, 29 Xueyuan Road, Beijing 100083, China; 2009220029@email.cugb.edu.cn (J.-H.X.); 2009210031@email.cugb.edu.cn (Y.Y.); 3009230008@email.cugb.edu.cn (G.-Y.W.)

<sup>2</sup> State Key Laboratory of Geological Processes and Mineral Resources, China University of Geosciences, Beijing 100083, China

<sup>3</sup> Taiwan Gemmological Research Center and Laboratory, 6th Floor, No. 92, Section 1, Zhongshan North Road, Zhongshan District, Taipei 10444, Taiwan; tgi.atc.lab@gmail.com

\* Correspondence: yuxy@cugb.edu.cn

**Abstract:** The homomorphic substitution of the garnet group is common in nature. Two rare color-changing andradite garnets are studied in this paper. One color changes from yellowish-green in the presence of daylight to maroon under incandescent light; the other color changes from brownish yellow to brownish red. In this study, conventional gemological instruments, infrared (IR) spectroscopy, ultraviolet–visible–near infrared (UV–Vis–NIR) spectroscopy, Raman spectroscopy, and electron probe microanalysis (EPMA) were used to explore the gemology and coloration mechanisms of color-changing garnets. Experiments revealed that the color-changing gemstones in the study are andradite garnets. There are two transmission windows in the UV–Vis spectrum: the red region (above 650 nm) and the green region (centered at 525 nm). The chemical compositional analysis indicates that the samples are very low in Cr (<1 ppm) and high in Fe<sup>2+</sup> (from 2.31 wt.% to 4.66 wt.%). The combined spectra and chemical compositional analysis show that Fe<sup>2+</sup> is the main cause of the color change. Based on the IR spectrum (complex water peaks), UV–Vis–NIR spectrum (similar to that of Namibian andradite garnet), and chemical compositional analysis (low Cr content), it is concluded that color-changing andradite may be related to skarn rock genesis.

**Keywords:** color-changing andradite; coloration mechanisms; chemical composition; spectroscopic analysis



**Citation:** Xu, J.-H.; Yu, X.-Y.; Shen, M.; Yan, Y.; Wang, G.-Y. Explaining Color Change in Gem-Quality Andradite Garnet. *Crystals* **2024**, *14*, 180. <https://doi.org/10.3390/cryst14020180>

Academic Editor: Vladislav V. Gurzhiy

Received: 30 January 2024

Revised: 6 February 2024

Accepted: 7 February 2024

Published: 11 February 2024



**Copyright:** © 2024 by the authors. Licensee MDPI, Basel, Switzerland. This article is an open access article distributed under the terms and conditions of the Creative Commons Attribution (CC BY) license (<https://creativecommons.org/licenses/by/4.0/>).

## 1. Introduction

There are many previous studies on color-changing garnets, most of which are aluminum garnets [1–3], while color-changing calcic garnets are rarely studied [4]. There is no systematic study on the coloration mechanism of color-changing andradite garnets, although color-changing andradite garnets were first reported in 2000, and there is a general gemological study in [5]. We stumbled upon two color-changing andradites on the market that have fascinating colors. To the best of our knowledge, the chemical composition of this type of color-changing garnet has never been reported before, and the study of color-changing andradite garnets is an important contribution to gemology. It also provides a theoretical basis for finding more color-changing andradite garnets to meet the market demand.

Garnet is an insular silicate mineral with the spatial group Oh10-Ia3d,  $a_0 = 1.459\text{--}1.248$  nm, and  $Z = 8$ . Its general chemical formula is  $A_3B_2[SiO_4]_3$ , where A represents a bivalent cation, such as Mg<sup>2+</sup>, Fe<sup>2+</sup>, Mn<sup>2+</sup>, and Ca<sup>2+</sup>, and B represents trivalent cations, mostly Al<sup>3+</sup>, Cr<sup>3+</sup>, Fe<sup>3+</sup>, Ti<sup>3+</sup>, Cr<sup>3+</sup>, V<sup>3+</sup>, and Zr<sup>3+</sup>. Compared with other bivalent ions, calcium has a larger ionic radius, so it is difficult to form isotropy with other bivalent ions. According to this, garnet can be divided into two categories: pyrospite series and calcarenite series.

In gemology, the difference between the color of a gemstone in daylight and under incandescent light is called the alexandrite-like effect. Many gemstones naturally change

color, such as alexandrite [6], spinel [7], sapphire [8], fluorite [9], and garnet [10]. The color-changing effect of gemstones is usually attributed to  $\text{Cr}^{3+}$  and  $\text{V}^{3+}$ , but there are exceptions. For example, Wang Zimin et al. [7], in their study on color-changing spinel, attributed Co ions and Fe ions to the color-changing effect.

The UV–Vis spectra of 10 color-changing pyrope–spessartine garnets were studied in 2021, and it was concluded that  $\text{Cr}^{3+}$  and  $\text{V}^{3+}$  were the main causes of the color change [2]. Twenty-four color-changing pyrope–spessartine garnets from Madagascar exhibited the alexandrite-like effect caused by  $\text{V}^{3+}$  [10]. In contrast, after studying color-changing pyrope–spessartine garnets, Yan concluded that the color-changing effect is the result of  $\text{Cr}^{3+}$  in the garnets [1]. Brunning has reported a color-changing grossular garnet and attributed the alexandrite-like effect to Cr and/or Fe [6]. Shen and Ye have reported a garnet exhibiting a tri-color change and concluded that the garnet was V dominant, with Mn, Fe, and Cr synergistically inducing the alexandrite-like effect [3]. Together, these previous studies suggest that there are four main explanations for the color genesis of color-changing garnets: The first is that the color-changing effect is caused by both  $\text{Cr}^{3+}$  and  $\text{V}^{3+}$  [2,3,11,12]. The second is that the alexandrite-like effect is mainly caused by  $\text{V}^{3+}$  [13,14]. The third is that the color-changing effect is mainly caused by  $\text{Cr}^{3+}$  [1,6,15,16]. The fourth is that the alexandrite-like effect is mainly caused by Fe [3,5]. The alexandrite-like effect of the samples studied in this paper is mainly  $\text{Fe}^{2+}$  chromogenic. This paper investigates the mechanism of the color change by analyzing the spectra, chemical compositions, and basic gemology of the samples.

## 2. Materials and Methods

### 2.1. Sample Description

In this study, the two color-changing andradite garnets are named G-1 (pear cut; size: 9.84 mm × 6.19 mm × 4.29 mm) and G-2 (emerald cut; size: 7.07 mm × 6.50 mm × 4.14 mm). G-1 weighs 1.81 carats, and its color changes from yellowish-green (Figure 1A) in the presence of daylight to maroon (Figure 1B) under incandescent light. G-2 weighs 1.83 carats, and its color changes from brownish yellow (Figure 1A) in the presence of daylight to brownish red (Figure 1B) under incandescent light.

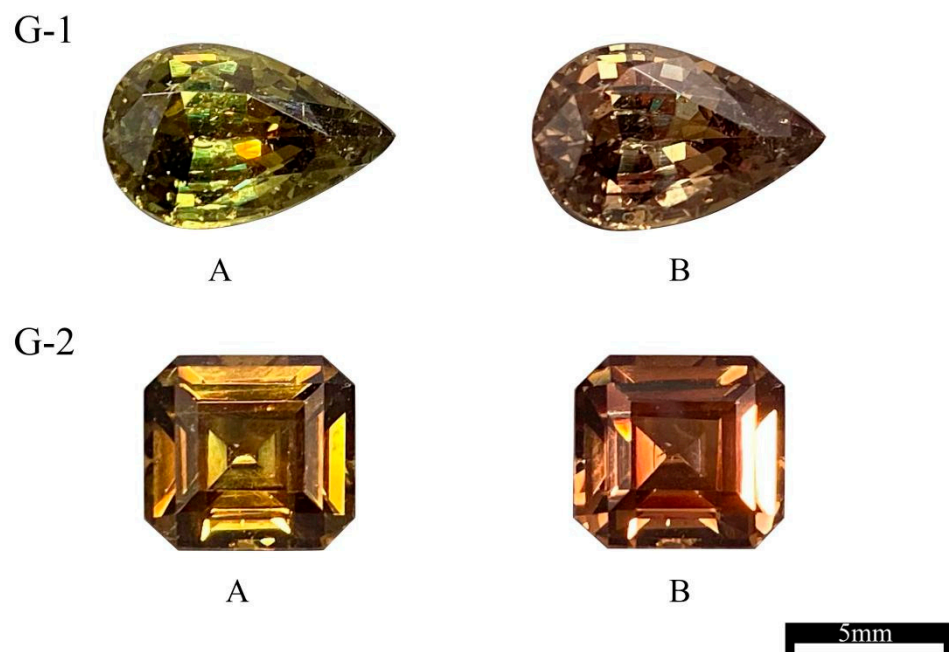


**Figure 1.** Photographs of specimens of color-changing garnets. Picture (A) was taken under standard D65 light; picture (B) was taken under standard A light.

## 2.2. Fourier-Transform Infrared (FTIR) Spectroscopy

FTIR spectroscopy was conducted at the Gemological Experimental Teaching Center at China University of Geosciences (Beijing, China). The instrument we used in the experiments was a BRUKER Tensor 27 (Bremen, Germany), a Fourier-transform infrared spectrometer.

The settings of the instrument were as follows: in the reflection mode, the scanning range was 400–1200  $\text{cm}^{-1}$ ; in the transmission mode, the scanning range was 2800–4000  $\text{cm}^{-1}$ ; power supply: 85–265 V; power supply frequency: 47–65 Hz; resolution: 4  $\text{cm}^{-1}$ ; grating setting: 6 mm; runtime: 30 s per scan; number of sample scans: 32. Based on the consensus that garnet is isotropic, randomly oriented crystals were tested, as the properties are constant in all directions.

## 2.3. UV–Vis–NIR Spectroscopy

UV–Vis–NIR spectroscopy was conducted at the Gemological Experimental Teaching Center at China University of Geosciences (Beijing, China). In different crystal structures, different types of electrons exhibit different activity characteristics, resulting in different electromagnetic radiation reactions of the mineral.

The UV–Vis–NIR spectra were measured using a GEM-3000 jewelry detector. The test conditions were as follows: wavelength range: 400–1000 nm; slit width: 2 nm; integration time: 170 ms; average number of times: 7; and the standard whiteboard was used to calibrate the detector before testing.

## 2.4. Raman Spectroscopy

Raman spectra were generated at the Gemological Experimental Teaching Center at China University of Geosciences (Beijing, China). The Raman spectra of the samples were generated using an HR-Evolution micro-Raman spectrometer. The test conditions were as follows: reflection mode; 532 nm wavelength laser; spectral range: 100–2000  $\text{cm}^{-1}$ ; and integration time: 3 s.

## 2.5. Electron Probe Microanalysis

EPMA was conducted at the Key Laboratory of Metallogeny and Mineral Assessment, Institute of Mineral Resources, Chinese Academy of Geological Science (CAGS, Beijing, China). The chemical compositions of the andradites were determined using EPMA and a JXA-8230 instrument (Japan Electron, Akishima, Japan). The test conditions were as follows: acceleration voltage: 15 kV; current: 20 nA; beam diameter: 5  $\mu\text{m}$ ; and the element peaks and background were measured at counting times of 10 s and 5 s, respectively. NaAlSi<sub>2</sub>O<sub>6</sub> (NaK $\alpha$ , TAP); Mg<sub>2</sub>SiO<sub>4</sub> (MgK $\alpha$ , TAP); Al<sub>2</sub>O<sub>3</sub> (AlK $\alpha$ , TAP); Al<sub>2</sub>SiO<sub>4</sub>(F,OH)<sub>2</sub> (FK $\alpha$ , TAP); KNbO<sub>3</sub> (KK $\alpha$ , PETJ); CaSiO<sub>3</sub> (CaK $\alpha$ , PETJ); SiO<sub>2</sub> (SiK $\alpha$ , PETJ); Fe<sub>3</sub>O<sub>4</sub> (FeK $\alpha$ , LIF); TiO<sub>2</sub> (TiK $\alpha$ , LIF); Ca<sub>5</sub>(PO<sub>4</sub>)<sub>3</sub> (PK $\alpha$ , PETJ); Cr<sub>2</sub>O<sub>3</sub> (CrK $\alpha$ , LIFH); MnO (MnK $\alpha$ , LIFH); NiO (NiK $\alpha$ , LIF); CaO<sub>6</sub>V<sub>2</sub> (VK $\alpha$ , LIFH); CoO (CoK $\alpha$ , PETH); and NaCl (ClK $\alpha$ , PETH) were used as standards. Matrix corrections were calculated using the ZAF method [17]. The detection limits for an individual element varied from 0.005 to 0.03 wt.%.

The structural formulae of the garnets were recalculated based on 12 O atoms per formula unit (apfu). Because garnet is isotropic and the samples have no color banding, three points of each sample were randomly selected for testing.

## 2.6. Laser Ablation–Inductively Coupled Plasma–Mass Spectrometry

The in situ trace element analysis of the minerals was conducted using LA–ICP–MS at the Mineral Micro Zone Analysis Laboratory of the OEDC, College of Resources and Environmental Engineering, Hefei University of Technology. The laser ablation system was a CetacAnalyte HE, and the ICP–MS was an Agilent 7900, with helium as the carrier gas and argon as the compensation gas to regulate the sensitivity during the laser ablation process, and the two gases were mixed through a T-connector before entering the ICP. Each piece of time-resolved analytical data consisted of 40 s of a blank signal and 40 s

of a sample signal. The off-line processing of the analyzed data (including the selection of the sample and blank signals, instructions for the sensitivity drift correction, and elemental content) was conducted using the software Spotanalysis (in-house laboratory software). The detailed instrumental operating conditions and data processing were the same as those in [18,19]. The minerals' trace element contents were quantitatively calculated using multiple reference glasses (NIST610, NIST612, and BCR-2G) as multiple external standards and without an internal standard [20]. The recommended values for the elemental contents in the standard glasses were according to those in the GeoReM database (<http://georem.mpch-mainz.gwdg.de/>). Four points per sample were selected for testing.

### 3. Results and Discussion

#### 3.1. Conventional Gemological Characteristics

Sample G-1 has a adamantine luster that is transparent and cracked and a cracked-surface grease luster, with  $RI > 1.78$ , a specific gravity of 3.81, and no reaction under a Chelsea filter. There are needle inclusions and stress cracks (Figure 2a), fluid inclusions (Figure 2b), and fingerprint inclusions (Figure 2c) under a  $40\times$  gemstone microscope. Sample G-1 appears yellowish-green under simulated natural light (D65 light) and maroon under simulated incandescent light (A light).

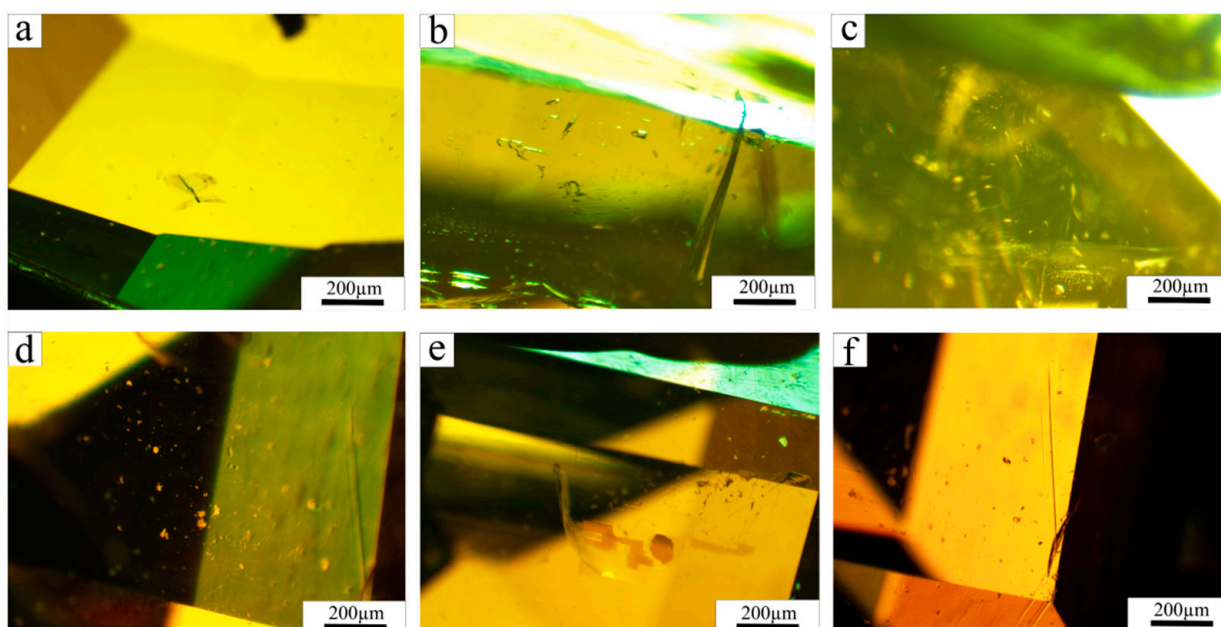


**Figure 2.** Internal inclusions in two samples at  $40\times$  magnification: (a) needle inclusions and stress cracks; (b) fluid inclusions; (c) fingerprint inclusions; (d) white spot-like inclusions; (e) brown flaky inclusions; (f) growth lines.

Sample G-2 has a adamantine luster that is transparent, with  $RI > 1.78$ , a specific gravity of 3.80, and no reaction under a Chelsea filter. There are white spot-like inclusions (Figure 2d), brown flaky inclusions (Figure 2e), and growth lines (Figure 2f) under a  $40\times$  gemstone microscope. Sample G-2 appears brownish yellow under simulated natural light (D65 light) and brownish red under simulated incandescent light (A light).

Samples G-1 and G-2 were inert under long-wavelength ultraviolet fluorescence (LWUV) at 365 nm and short-wavelength ultraviolet fluorescence (SWUV) at 254 nm, which is mainly because they are rich in Fe. It is well known that Fe is a fluorescence quencher.

Flat growth lines were observed under a  $40\times$  gemstone microscope, while andradite garnet has this characteristic [7]. The standard gemological properties of the specimens are listed in Table 1.

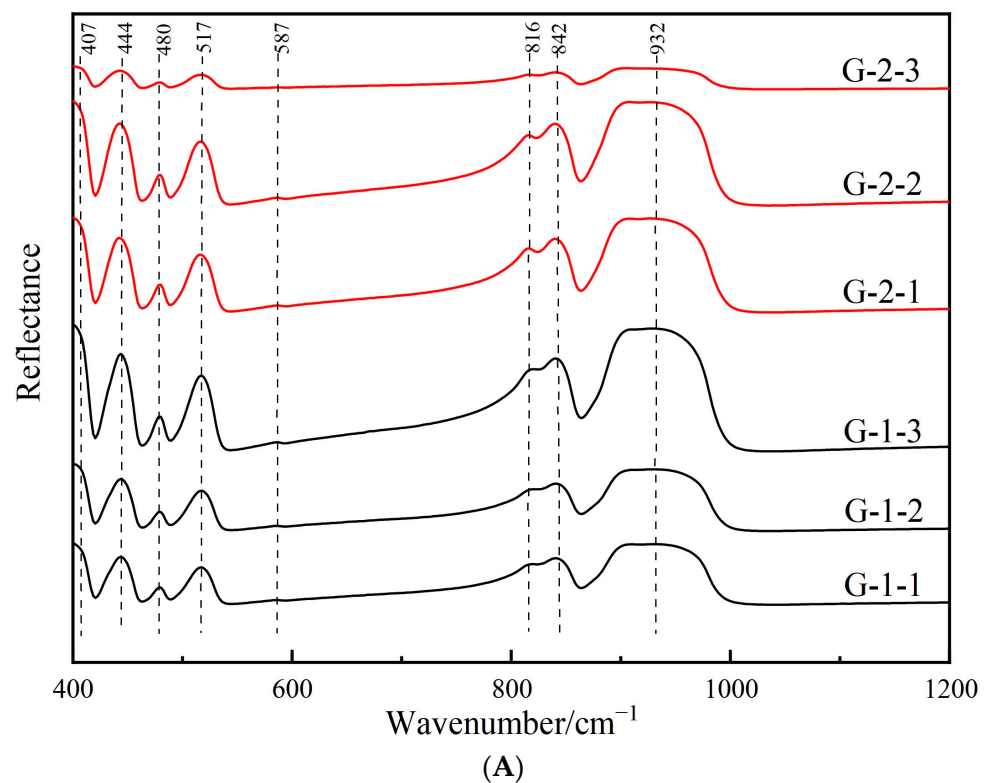
**Table 1.** Gemological properties of specimens.

Sample Number	G-1	G-2
Color	Yellowish-green in daylight and maroon under incandescent light	Brownish yellow in daylight and brownish red under incandescent light
Luster	Adamantine	Adamantine
Clarity	Many fluid inclusions	Obvious inclusions can be seen under the table
Specific gravity	3.81	3.80
Fluorescence	Inert	Inert
Chelsea filter	No reaction	No reaction
Refractive index	RI > 1.78	RI > 1.78
Internal features	Fissures, fingerprint inclusions, dark inclusions, visible growth lines, and parallel gas–liquid inclusions	Fingerprint inclusions and stress cracks, white point inclusions, fluid inclusions, light brown inclusions, and visible growth lines

### 3.2. FTIR Spectroscopy

For different subspecies of garnet, the fingerprint region of their infrared spectra are significantly different, so they can be identified according to the fingerprint region's infrared spectral absorption peak characteristics.

The infrared spectra of the samples (400–1200  $\text{cm}^{-1}$ ), shown in Figure 3A, were generated in the reflection mode. The main absorption peaks of the two samples are located at 407, 444, 480, 517, 587, 816, 842, and 932  $\text{cm}^{-1}$ . The vibration peaks at 932, 842, and 816  $\text{cm}^{-1}$  represent asymmetric stretching vibrations of  $[\text{SiO}_4]^{4-}$ ; the vibration peaks at 480, 517, and 587  $\text{cm}^{-1}$  represent the bending vibrations of  $[\text{SiO}_4]^{4-}$ ; and the peaks at 444 and 407  $\text{cm}^{-1}$  are absorption bands associated with  $\text{Ca}^{2+}$  vibrations [21,22].

**Figure 3.** Cont.

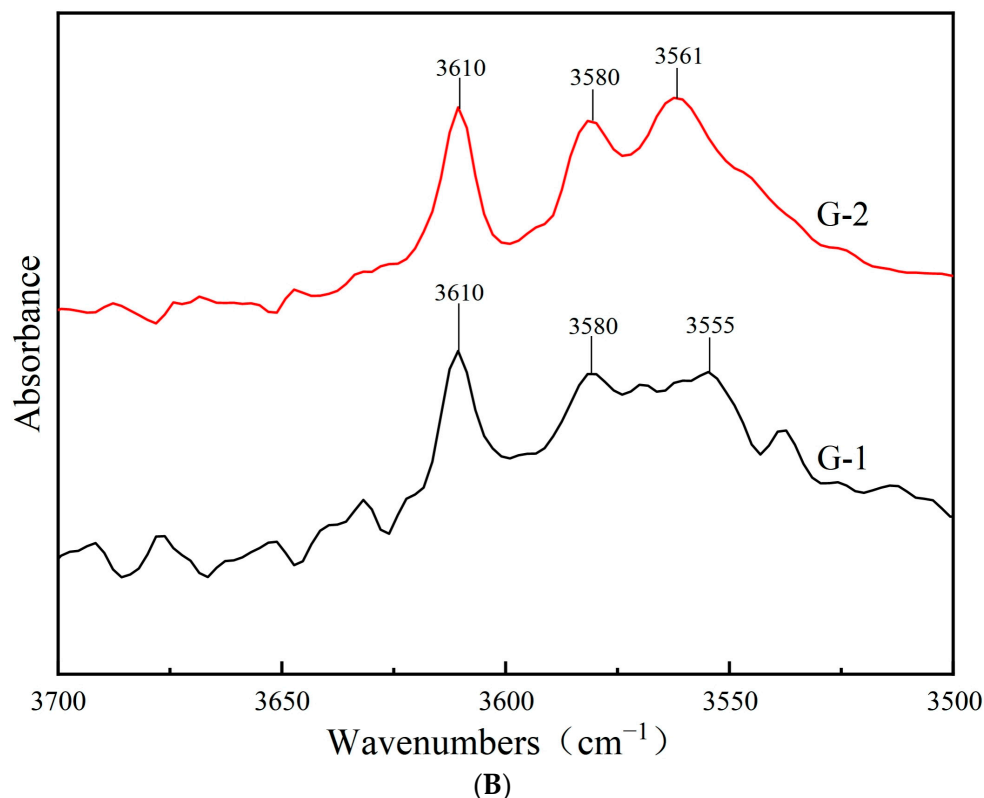


**Figure 3.** (A) The FTIR spectra of the samples in the reflection mode in the range 400–1200  $\text{cm}^{-1}$ ; (B) the FTIR spectra of the samples in the transmission mode in the range 3500–3700  $\text{cm}^{-1}$ .

Although garnet is an anhydrous mineral, water-related peaks were still observed in the mid-infrared spectra in previous studies [23]. Some of the water-related peaks of andradite garnets derived from different origins are listed in Table 2. The mid-infrared spectra of the two samples investigated over the range of fundamental water molecule stretching vibrations (3500–3700  $\text{cm}^{-1}$ ) in the transmission mode are shown in Figure 3B. The main water molecule absorption bands are at 3555  $\text{cm}^{-1}$ , 3561  $\text{cm}^{-1}$ , 3580  $\text{cm}^{-1}$ , and 3610  $\text{cm}^{-1}$ . In particular, the prominent absorption bands at about 3555  $\text{cm}^{-1}$  and 3561  $\text{cm}^{-1}$  suggest the well-known hydrogarnet substitution  $(\text{SiO}_4)^{4-} \leftrightarrow (\text{H}_4\text{O}_4)^{4-}$  [24]. The absorption bands at about 3580  $\text{cm}^{-1}$  and 3610  $\text{cm}^{-1}$  are caused by other kinds of  $\text{OH}^-$  incorporation than just the substitution  $(\text{SiO}_4)^{4-} \leftrightarrow (\text{H}_4\text{O}_4)^{4-}$  [24]. This mid-infrared result indicated that the samples contain water, suggesting that color-changing garnet contains a small amount of structural water, which is related to its formation process with water. The mid-infrared spectrum shows a more intense characteristic absorption band at 3561  $\text{cm}^{-1}$  for G-2, suggesting that G-2 contains more water and may have formed at lower temperatures [25]. Ilaria Adamo et al. [26] stated that andradites derived from skarns exhibit more complex water peaks than andradites derived from serpentinites, and our spectra are very similar to those of the andradite derived from the skarn, as reported by [26]; therefore, the samples may have formed in association with skarns.

**Table 2.** Some of the water-related peaks in the FTIR spectra of andradite garnets.

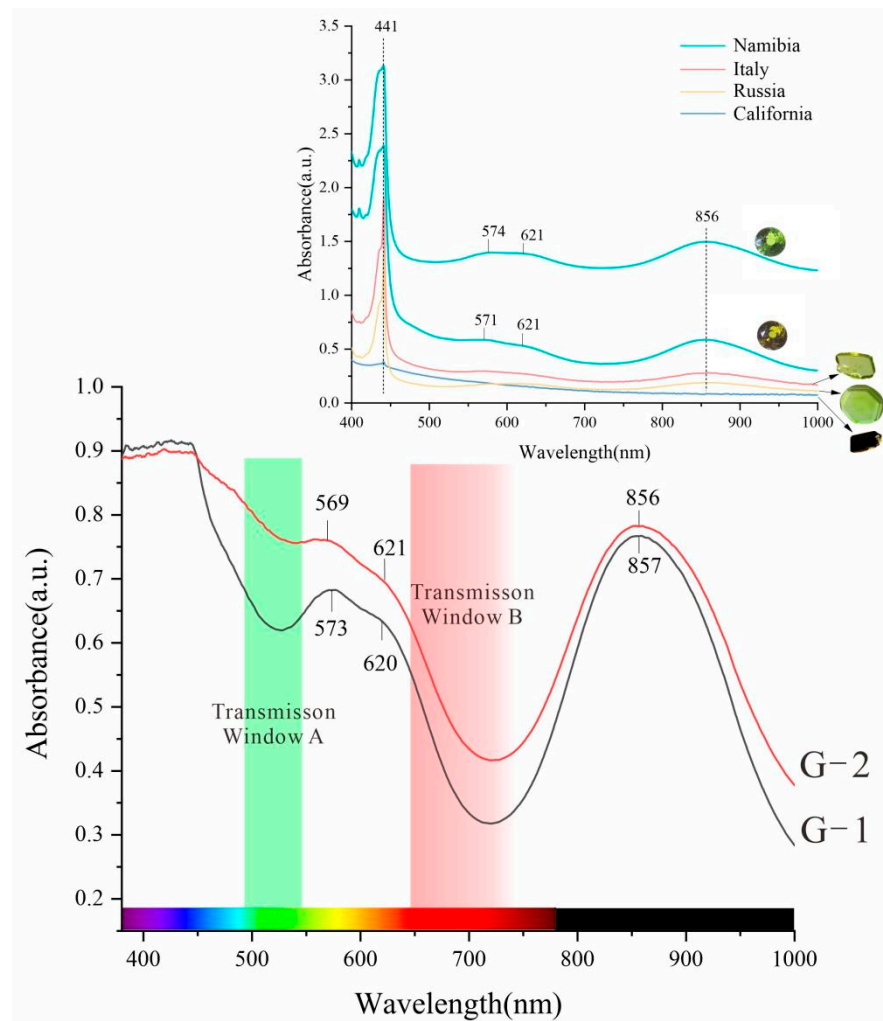
Locality	Water-Related Peaks	Data Source
Russia	3562, 3604, and 3394 $\text{cm}^{-1}$	[21]
Bombay, India	3560 and 3610 $\text{cm}^{-1}$	[25]
Rusinga Island	3530 and 3560 $\text{cm}^{-1}$	[25]
Stanley Butte, Arizona	Four resolved peaks between 3550 and 3630 $\text{cm}^{-1}$ and three shoulders between 3630 and 3700 $\text{cm}^{-1}$	[25]

Table 2. Cont.

Locality	Water-Related Peaks	Data Source
Madagascar	3560, 3580, 3610, and 3630 $\text{cm}^{-1}$	[26]
Namibia	3562, 3581, 3611, and 3631 $\text{cm}^{-1}$	[26]
Pakistan	3564 and 3605 $\text{cm}^{-1}$	[26]
Iran	3563 and 3605 $\text{cm}^{-1}$	[26]
Russia	3558 $\text{cm}^{-1}$	[26]
Valmalenco	3562 and 3604 $\text{cm}^{-1}$	[26]
Valmalenco, Italy	3563 $\text{cm}^{-1}$	[27]

### 3.3. UV–Vis–NIR Spectroscopy

The UV–Vis–NIR spectral test results of the two color-changing garnets are shown in Figure 4. To investigate the coloration mechanism of the color-changing andradites, data from previous studies of different countries' andradites (one is black and the others are yellow–green) were added as a comparison. Overall, the UV–Vis–NIR spectral trend from 500 nm to 1000 nm is quite similar to that of the Namibian andradite, but the spectra for the samples lack the absorption peak at 441 nm caused by  $\text{Fe}^{3+}$ .



**Figure 4.** UV–Vis–NIR spectra of the color-changing samples and andradite garnets without the alexandrite-like effect. (Data for different countries were obtained from <http://minerals.gps.caltech.edu/FILES/Visible/Garnet/Index.html>, accessed on 5 February 2024).

The G-1 spectrum displayed two broad bands at around 573 nm and 857 nm and a weak absorption band centered at around 620 nm; the G-2 spectrum displayed two strong absorption bands centered at around 569 nm and 856 nm and a weak absorption band centered at around 621 nm. As a consequence, two transmission windows in the green (centered at 525 nm) and red (above 650 nm) regions of the visible spectrum were responsible for the color-changing effect of the two andradite garnets. When the transmittance of the two regions is almost the same, the color of the gem is determined by the external light source. The absorptions at 573 nm and 569 nm correspond to the spin-forbidden transitions ( ${}^5E_g \rightarrow {}^3T_{1g}$  and  ${}^5E_g \rightarrow {}^3E_{1g}$ , respectively) of eightfold-coordinated high-spin  $Fe^{2+}$ , and  $Fe^{3+}$  may have a contribution to these absorption bands [25,28–31]. The unusual high-intensity spin-forbidden optical transitions of eightfold-coordinated  $Fe^{2+}$  cause many optical transitions in the green–yellow part of the visible spectrum and leave two strong transmission windows in the green and red spectral regions. Namibian garnet has a lower absorption peak around 573 nm relative to the samples and lacks a transmission window in the red zone, which is why it does not produce an alexandrite-like effect. Although LA-ICP-MS was not used to test for Cr in the samples, some scholars have studied the UV-Vis absorption spectra of Madagascar and Italian demantoids, and only samples containing Cr showed an absorption band at 620 nm [16]. Very small amounts (<1 ppm) of Cr may be present in the samples. The weak absorption bands at 620 nm and 621 nm are both ascribable to Fe, and the spin-forbidden transitions of  $Cr^{3+}$  ( ${}^4A_{2g} \rightarrow {}^4T_{1g}$ ) may have a slight contribution to these absorption bands [5,13,26,30,32]. The  $Fe^{2+}$  spin-forbidden transition ( ${}^5E(D) \rightarrow {}^3T_1(H)$ ) produces a broad absorption band in the visible-light range 550–650 nm, leading to two transmittance regions on both sides, which show a yellowish green to brown alexandrite-like effect along with the change in the spectral power distribution of the light source. Moreover, a broad band at about 856 nm was due to octahedral  $Fe^{3+}$  [25,28,33].

The wide absorption bands at 569 nm and 573 nm are caused by  $Fe^{2+}$ , and it is the main reason for the alexandrite-like effect. Most color-changing gems show similar characteristics in their UV-Vis spectra. They all have strong absorptions in the blue–violet region and the orange–yellow region, and the wide absorption band’s center must be within the range 562–578 nm to produce the color-changing effect [34]. Unlike other common color-changing gemstones, where the strong absorption bands in the green spectral region are caused by  $Cr^{3+}$  at two different crystal sites and are, thus, responsible for the alexandrite-like effect, in andradite garnets, the strong absorption bands are due to  $Fe^{2+}$ . Some previous studies on the UV-Vis analysis of color-changing garnets are listed in Table 3. It can be concluded from the UV-Vis-NIR spectra that the intensity of the absorption peak at 573 nm for G-1 is greater than that of the absorption peak at 573 nm for G-2, and this is consistent with the G-1 color-changing effect, which is more readily observed by the naked eye.

**Table 3.** Previous studies on the UV-Vis analysis of color-changing garnets.

Type	Analysis of UV-Vis Spectra	Data Source
Pyrope–spessartine garnet	The absorption band centered at about 571 nm is the result of $Cr^{3+}$	[1]
Pyrope–spessartine garnet	The absorption band centered at about 574 nm is caused by $Cr^{3+}$ and $V^{3+}$	[2]
Iron- and calcium-bearing manganic pyrope garnet	The absorption band centered at about 575 nm is the result of $V^{3+}$ and $Cr^{3+}$	[3]
Andradite	The absorption bands at about 575 nm and 610 nm are caused by Fe	[5]
Grossular garnet	The absorption band centered at about 600 nm is caused by $Cr^{3+}$	[6]
Pyrope–spessartine garnets	The absorption band centered at about 573 nm is caused by $V^{3+} \pm Cr^{3+}$	[6]
Pyrope–spessartine garnets	V is the main element of the color-changing effect	[10]

Table 3. Cont.

Type	Analysis of UV-Vis Spectra	Data Source
Pyrope–spessartine garnet	The absorption band centered at about 571 nm is the result of Cr <sup>3+</sup> and V <sup>3+</sup>	[11]
Pyrope garnet	V and Cr are the main elements of the color-changing effect	[12]
Pyrope–spessartine garnet	The wide absorption band centered at about 575 nm is caused by V <sup>3+</sup>	[13]
Spessartine garnet	The absorption band centered at about 585 nm is caused by V <sup>3+</sup>	[14]
Magnesium-rich spessartine garnet	The absorption band between 580 nm and 620 nm is caused by Cr	[15]
Grossular garnet	The absorption band centered at about 599 nm is the result of Cr <sup>3+</sup> and V <sup>3+</sup>	[34]
Pyrope–spessartine garnet	The absorption band centered at about 573 nm is caused by V <sup>3+</sup> and Cr <sup>3+</sup>	[35]
Almandine–pyrope garnet	The absorption bands at 573 nm and 618 nm are caused by Fe <sup>2+</sup>	[36]

### 3.4. Raman Spectroscopy

The homomorphic substitution of the garnet group is common, and the Raman spectra of different subspecies are different. Three points for each sample were selected for an in situ Raman spectral test, and all the test results were completely consistent. The Raman spectra are shown in Figure 5, and the main Raman shifts are shown in Table 4. Four Raman peaks (995.5, 873.5, 841.5, and 815 cm<sup>-1</sup>) between 800 and 1000 cm<sup>-1</sup> are generated by [SiO<sub>4</sub>]<sup>4-</sup> stretching vibrations. The five Raman peaks between 400 and 600 cm<sup>-1</sup> (576, 552, 515, 492.5, and 452 cm<sup>-1</sup>) are generated by the bending vibrations of [SiO<sub>4</sub>]<sup>4-</sup>; the Raman peak between 300 and 400 cm<sup>-1</sup> is caused by the rotational vibrations of [SiO<sub>4</sub>]<sup>4-</sup>, and the Raman peak between 150 and 300 cm<sup>-1</sup> is caused by the translational vibrations of Ca<sup>2+</sup> and the [SiO<sub>4</sub>]<sup>4-</sup> tetrahedron in the garnet [37]. The Raman spectra of the samples are basically consistent with those of the andradite garnets from Russia and Madagascar and the RRUFF standards, and it can be determined that the sample is andradite garnet.

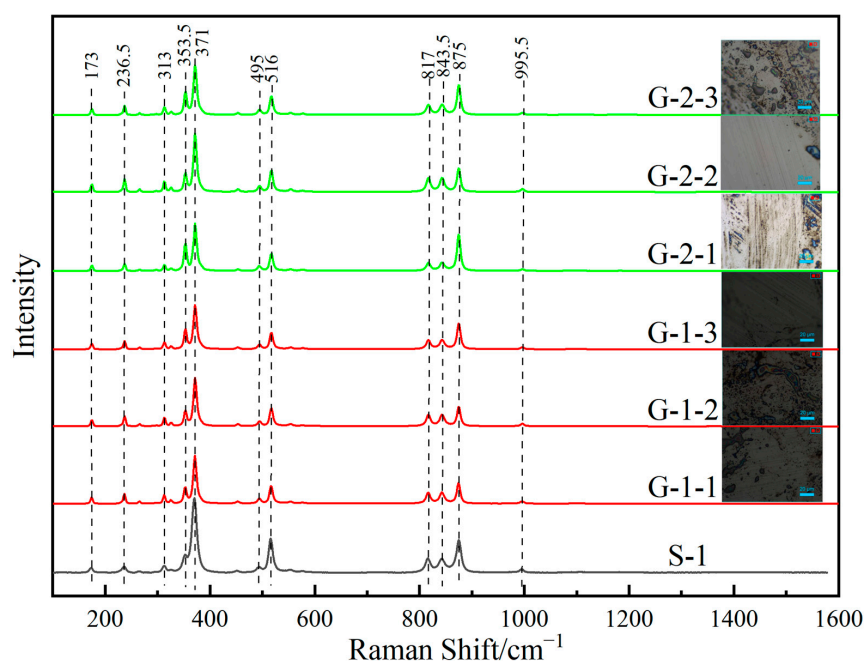


Figure 5. Raman spectra of color-changing andradite garnets. S-1 is the standard of the andradite garnet in RRUFF.

**Table 4.** Raman shifts ( $\text{cm}^{-1}$ ) of samples.

Peak Position Attribution [37]	Stretching Vibrations of $[\text{SiO}_4]$				Bending Vibrations of $[\text{SiO}_4]$					Rotational Vibrations of $[\text{SiO}_4]$				Translational Vibrations of $\text{Ca}^{2+}$ and $[\text{SiO}_4]$			
	$\nu_3$	$\nu_1$	$\nu_3$	$\nu_3$	$\nu_4$	$\nu_4$	$\nu_4$	$\nu_4$	$\nu_2$								
Samples	995.5	873.5	841.5	815	576	552	515	492.5	453	369	350.5	323	311	298	266	236.5	173
Andradite from Russia [17]	994.5	873.5	841.5	815	576	552	515	492	451	369	351	323	310.5	295	263	234.5	172
Andradite from Madagascar [38]	996	874	841	815	576	555	515	493	454	371	352	324	312	304	266	236	174

### 3.5. Chemical Compositional Characteristics

The major and minor elemental compositions of the color-changing andradite samples expressed in oxides and the formulae obtained from individual crystals by EPMA are presented in Table 5. To study more accurately the contents of the chromogenic elements in the samples, trace element testing by LA-ICP-MS was carried out. The test results are shown in Table 6. The end-element component contents of each test point in Table 5 (combined with Table 6) were projected onto an  $\text{Fe}^{3+} - \text{Al}^{3+} - \text{Cr}^{3+}$  triangle diagram to visually determine the subspecies of this garnet. The subspecies of the samples are plotted in Figure 6. Andradite garnet data from well-known producing regions around the world are added to Figure 6 for comparison and cast points. From Figure 6, it can be concluded that skarn-type andradite garnets are mostly located in non-colored areas at very low Cr contents ( $\text{Cr}^{3+} < 0.25$  in the three-phase diagram), while serpentinite-type andradite garnets are located in gray areas at high Cr contents ( $\text{Cr}^{3+} \geq 0.25$  in the three-phase diagram). From the three-phase diagram, we can roughly distinguish whether the andradite garnet is the serpentinite type or skarn type. The samples described in the text are located in non-colored areas in the three-phase diagrams, which may be related to skarn rock genesis.

**Table 5.** Electron probe microanalyses of andradites, first provided as weight percentages of elements and then recalculated based on 12 anions.

Sample EPMA	G-1-1	G-1-2	G-1-3	G-2-1	G-2-2	G-2-3
$\text{Al}_2\text{O}_3$	0	0	0.016	0.002	0.01	0.011
$\text{MgO}$	0.032	0.034	0.075	0.047	0.052	0.079
$\text{Na}_2\text{O}$	0.042	0.023	0.17	0.061	0.026	0
$\text{K}_2\text{O}$	0.028	0.002	0.052	0.014	0.015	0.019
$\text{CaO}$	32.337	32.253	32.29	32.028	32.131	31.974
$\text{Cr}_2\text{O}_3$	0.042	0	0.047	0.009	0	0.047
$\text{SiO}_2$	38.803	38.55	37.38	37.299	37.038	36.599
$\text{P}_2\text{O}_5$	0.026	0.01	0.049	0.013	0.013	0.033
$\text{V}_2\text{O}_3$	0	0	0	0.024	0.024	0.111
$\text{MnO}$	0	0	0.016	0	0.009	0
$\text{Fe}_2\text{O}_3$	23.655	23.428	25.749	24.523	25.323	25.380
$\text{FeO}$	4.66	4.552	2.310	3.206	2.852	2.646
$\text{TiO}_2$	0.028	0	0	0.049	0.002	0.026
$\text{CoO}$	0.059	0.075	0.024	0.025	0.035	0.049
Total	99.708	98.927	98.177	97.301	97.530	96.974
$\text{P}^{5+}$	0.002	0.001	0.004	0.001	0.001	0.002
$\text{Si}^{4+}$	3.253	3.256	3.184	3.207	3.182	3.164
$\Sigma$	3.255	3.257	3.188	3.208	3.183	3.166
$\text{Al}^{3+}$	0	0	0.002	0	0.001	0.001
$\text{Cr}^{3+}$	0.003	0	0.003	0.001	0	0.003
$\text{V}^{3+}$	0	0	0	0.002	0.002	0.008
$\text{Fe}^{3+}$	1.492	1.489	1.65	1.587	1.637	1.651
$\text{Ti}^{3+}$	0.002	0	0	0.003	0	0.002
$\Sigma$	1.497	1.489	1.655	1.593	1.64	1.665
$\text{Mg}^{2+}$	0.004	0.004	0.01	0.006	0.007	0.01
$\text{Na}^+$	0.007	0.004	0.028	0.01	0.004	0
$\text{K}^+$	0.003	0	0.006	0.002	0.002	0.002
$\text{Ca}^{2+}$	2.904	2.919	2.947	2.95	2.957	2.962
$\text{Mn}^{2+}$	0	0	0.001	0	0.001	0
$\text{Fe}^{2+}$	0.326	0.322	0.165	0.231	0.205	0.191
$\text{Co}^{2+}$	0.004	0.005	0.002	0.002	0.002	0.003
$\Sigma$	3.248	3.254	3.159	3.201	3.178	3.168
End-member (%)						
Adr	84.16	84.06	87.71	86.67	88.64	89.30
Others	15.84	15.94	12.29	13.33	11.36	10.70

**Table 6.** Trace element compositions (in ppm) of andradite samples analyzed using LA-ICP-MS. Bdl = below detection limit.

Element	G-1A	G-1B	G-1C	G-1D	G-2A	G-2B	G-2C	G-2D
Mg	283	294	331	356	337	337	343	351
Al	76.4	43.3	128	243	40.5	39.2	40.5	38
Sc	2.47	2.46	2.47	2.72	2.43	2.68	2.37	2.52
Ti	1.2	2.07	6.95	9.63	Bdl	Bdl	Bdl	1.63
V	Bdl	Bdl	0.119	0.182	Bdl	Bdl	Bdl	Bdl
Cr	Bdl							
Mn	128	153	167	162	49.2	49.6	49.9	51.1
Co	0.253	0.217	0.366	0.334	0.235	0.147	0.175	0.147
Ni	1.09	1.17	1.42	1.22	Bdl	0.239	Bdl	Bdl
Ce	1.79	0.642	1.18	2.93	Bdl	Bdl	Bdl	Bdl
Nd	0.672	Bdl	Bdl	1	Bdl	Bdl	Bdl	Bdl
Fe	139,367	139,056	138,360	139,617	138,809	139,397	139,465	138,104
Ga	35.1	34.2	42.6	76.9	19.4	20.9	20	19.3
Sn	66.1	68.1	72.1	78.9	42.7	46.4	47.1	47.3

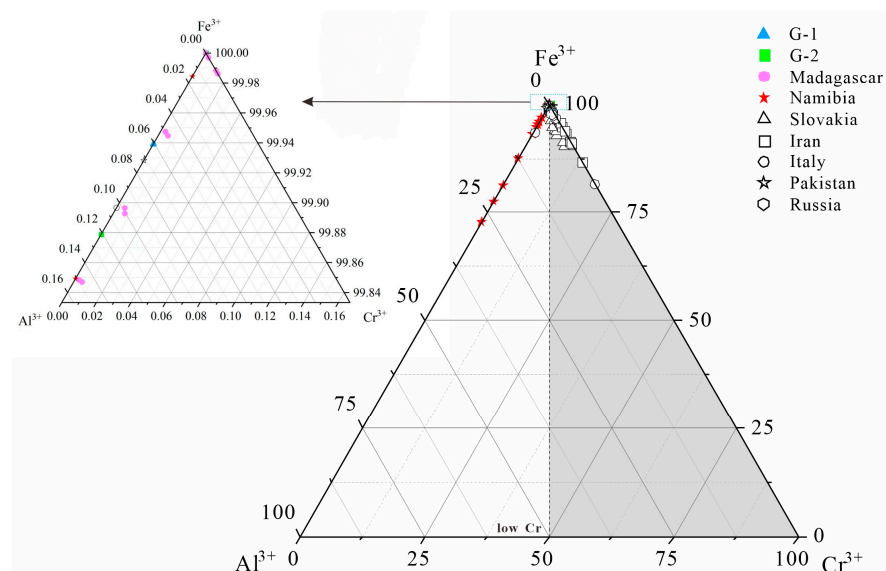


**Figure 6.** Ternary  $\text{Fe}^{3+}$ – $\text{Al}^{3+}$ – $\text{Cr}^{3+}$  (wt.%) plots of andradites derived from different origins [16,33,39–43]. Blue triangles and green squares represent G-1 and G-2, respectively, and purple circles and red stars indicate andradites derived from skarn, while blank legend indicates andradites derived from serpentine. White triangular area indicates that the content of  $\text{Cr}^{3+}$  is below 0.25 in the three-phase diagram.

In the EPMA test, the major elements in both samples were Si, Ca, and Fe, and the trace elements were Al, Mg, Na, K, Cr, P, V, Mn, Ti, and Co (Table 5). Because the EPMA yielded data for all the FeO, calculations were made for  $\text{Fe}^{2+}$  and  $\text{Fe}^{3+}$  according to the formula  $\text{Fe}_2\text{O}_3 = 2\text{FeO} + \text{O}_x$ .

The crystal formulae were quantitatively calculated based on the average chemical composition of the three experiments. The mineral composition of the G-1 garnet was calculated as andradite garnet (85.31%) + others (14.69%); its chemical formula is  $(\text{Mg}_{0.006}\text{Na}_{0.013}\text{K}_{0.003}\text{Co}_{0.004}\text{Fe}_{0.271}\text{Ca}_{2.923})(\text{Al}_{0.001}\text{Cr}_{0.002}\text{Ti}_{0.001}\text{Fe}_{1.544})(\text{Si}_{3.231}\text{P}_{0.002})\text{O}_{12}$ . The mineral composition of the G-2 garnet was calculated as andradite garnet (88.20%) + others (11.8%); its chemical formula is  $(\text{Mg}_{0.008}\text{Na}_{0.005}\text{K}_{0.002}\text{Co}_{0.002}\text{Fe}_{0.209}\text{Ca}_{2.956})(\text{Al}_{0.001}\text{Cr}_{0.001}\text{V}_{0.004}\text{Ti}_{0.002}\text{Fe}_{1.625})(\text{Si}_{3.184}\text{P}_{0.001})\text{O}_{12}$ . The qualitative EPMA analysis revealed that the samples are andradite garnets, which is consistent with the results of the Raman spectra. The total number of experimental EPMA data is fewer than 100 because of the presence of wa-

ter in the samples, as revealed by the infrared data. The total amount of G-2 is less than that of G-1, which is due to the fact that G-2 contains more structural water. The results of the EPMA chemical composition test show that the main components of the two samples are CaO and Fe<sub>2</sub>O<sub>3</sub>, which is consistent with those of andradite garnets studied in previous research, and that both samples contain trace elements, such as Co, Ti, and V. As can be seen from Table 6, the total amounts of the rare-earth elements in the samples are not high ( $\Sigma$ REE = 0.859–4.7 ppm), except for Ce and Nd; the amounts of the rest of the rare-earth elements are lower than the detection limit, and it is clear to see that the samples are enriched in light rare earths and deficient in heavy rare earths. This characteristic is similar to that of andradite garnets derived from most origins [16]. Unlike common andradite garnets, more Fe<sup>2+</sup> ions are contained in the color-changing garnets, and the contents of the Mn and V ions in the color-changing garnets are close to those of the Mn and V ions in the yellow–green andradite garnet with no alexandrite-like effect [16,39]. Mn and V are not major causes of color-changing andradite garnets.

The color of most garnets is derived from multiple color-producing elements (chromophores) [12]. The main chromophore elements are Fe, Ni, Cr, V, Mn, and Co, and trace amounts of the rare-earth elements Ce and Nd also affect the color of garnets [40]. According to Table 6, G-1 has a small amount of V (<1 ppm), and G-2 has an amount of V that is below the detection limit; both samples have amounts of Cr that are below the detection limit. The lowest level of Cr that causes the alexandrite-like effect in color-changing gemstones is 205 ppm [31]. The Cr contents of the samples were well below the minimum value. Table 6 shows that the Ce + Nd contents of both samples are less than 5 ppm, and neither Ce nor Nd is the main cause of the color change. The variation in the individual chromophores Cr<sup>3+</sup> and V<sup>3+</sup> is much stronger than that in Fe<sup>2+</sup> and Mn<sup>2+</sup> under different light sources, but the high content of Fe<sup>2+</sup> (6660–16,660 ppm) can also cause an obvious discoloration effect [12]. According to the calculated average element concentrations in Table 5, G-1 contains 29,939 ppm of Fe<sup>2+</sup>, and G-2 contains 22612 ppm of Fe<sup>2+</sup>; Fe<sup>2+</sup> concentrations below 6660 ppm and above 16,660 ppm both significantly reduce the alexandrite-like effect. This also explains the weak alexandrite-like effect of the samples described in the text. Combined with the UV–Vis–NIR spectra, these results suggest that the Fe element is the main reason for the color change in the andradite garnets.

#### 4. Conclusions

The samples have a adamantine luster that is transparent, with RI > 1.78, a specific gravity in the range 3.80–3.81, no reaction under a Chelsea filter, and abundant inclusions. The pear-cut sample is yellowish-green in D65 light and maroon in A light; the emerald-cut sample is brownish yellow in D65 light and brownish red in A light. According to the chemical compositional analysis, unlike common andradite garnets, color-changing garnets have a high content of Fe<sup>2+</sup>, and their contents of Cr and/or V (common elements leading to the alexandrite-like effect) and Ce + Nd are very low. In the UV–Vis–NIR spectra, the wide absorption band near 575 nm is produced by the spin-forbidden transition (<sup>5</sup>E<sub>g</sub> → <sup>3</sup>T<sub>1g</sub> and <sup>5</sup>E<sub>g</sub> → <sup>3</sup>E<sub>1g</sub>) of eightfold-coordinated high-spin Fe<sup>2+</sup>, leading to the emergence of transmission windows in the green (centered at 525 nm) and red (above 650 nm) regions, which is the main reason for the alexandrite-like effect of the color-changing andradite.

Combined with the complex structural water molecule absorption peaks (at 3631 cm<sup>−1</sup>, 3610 cm<sup>−1</sup>, 3580 cm<sup>−1</sup>, and 3561 cm<sup>−1</sup>) in the IR spectra, the UV–Vis–NIR spectral trend of the samples is highly similar to that of Namibian andradite garnet (having a very low Cr content), and the samples are located in the range of the skarn-type andradite garnet (Cr<sup>3+</sup> < 0.25) in the triple-phase diagrams; therefore, the samples are most likely produced in skarn. This is important for exploring more color-changing andradite garnets to meet the market demand.

**Author Contributions:** Conceptualization, J.-H.X. and X.-Y.Y.; methodology, J.-H.X. and X.-Y.Y.; software, J.-H.X.; validation, J.-H.X., Y.Y. and X.-Y.Y.; formal analysis, J.-H.X. and X.-Y.Y.; investigation, J.-H.X., X.-Y.Y. and G.-Y.W.; resources, M.S. and X.-Y.Y.; data curation, J.-H.X.; writing—original draft preparation, J.-H.X.; writing—review and editing, J.-H.X. and X.-Y.Y.; visualization, J.-H.X. and X.-Y.Y.; funding acquisition, X.-Y.Y. All authors have read and agreed to the published version of the manuscript.

**Funding:** This study was financially supported by a project from the China Geological Survey (DD20190379-88).

**Data Availability Statement:** The data presented in this study are available in this article.

**Acknowledgments:** We are very grateful to Ming-ke Wu and Yi Zhang for their help and comments. The authors also thank Zhe-yi Zhao and Yu-shu Yang for their valuable help.

**Conflicts of Interest:** The authors declare no conflicts of interest.

## References

1. Yan, X.; Yue, S.; Chen, S. Gemological Characteristics and Discoloration Mechanism of Color-Chang Pyrope-Spessartine Garnet. *Laser Optoelectron. Prog.* **2022**, *59*, 1333001.
2. Qiu, Y.; Guo, Y. Explaining Colour Change in Pyrope-Spessartine Garnets. *Minerals* **2021**, *11*, 865. [[CrossRef](#)]
3. Shen, Y.A.; Ye, P. Cause of Tri-colour Change Effect of a Rare Garnet. *J. Gems Gemmol.* **2018**, *20*, 17–23.
4. Supparat, P.; Apitchaya, B. A Rare Nearly Pure End-Member Grossular Garnet with Color-Change Effect. *Gems Gemol.* **2018**, *54*, 336.
5. Williams, C.; Williams, B. Colour-Change Andradite. *J. Gemmol.* **2021**, *37*, 562–564. [[CrossRef](#)]
6. Brunning, A. The Color of Alexandrite. *Am. Sci.* **2019**, *107*, 10.
7. Wang, Z.-m.; Mao, X.-t.; Yin, Z.-w.; Chen, C.; Cheng, T.-j. Study on the Spectral Characteristics and the Color-Change Effect of Spinel. *Spectrosc. Spectr. Anal.* **2022**, *42*, 3541–3545.
8. Wang, H.; Yu, X.-Y.; Liu, F.; Alam, M.; Wu, G.-C. Color Genesis and Compositional Characteristics of Color-Change Sapphire from Fuping, China. *Crystals* **2022**, *12*, 463. [[CrossRef](#)]
9. Houran, J.; Laurs, B.M. Fluorite impersonating blue color-change garnet. *Gems Gemol.* **2008**, *44*, 263.
10. Krzemnicki, M.S. Color-change in garnets from Madagascar: A comparison of colorimetric with chemical data. *J. Gemmol.* **2001**, *27*, 395–408. [[CrossRef](#)]
11. Liu, C.-h.; Chen, C.-y.; Shao, T.; Li, Z.-b.; Shen, A.H. UV-Vis Absorption Spectra and 3D Fluorescence Spectra Study of Color-Change Garnet with Red Fluorescence. *Spectrosc. Spectr. Anal.* **2020**, *40*, 2148–2152.
12. Sun, Z.; Palke, A.C.; Renfro, N.D.; Rizzo, J.M.; Hand, D.B.; Sanchez, D. Quantitative definition of strength of chromophores in gemstones and the impact on color change in pyralspite garnets. *Color Res. Appl.* **2022**, *47*, 1134–1154. [[CrossRef](#)]
13. Li, L.P.; Ye, D. Roles of Cr and V in color change effect of gemstones. *J. Gems Gemmol.* **2003**, *5*, 17–21.
14. Breitzmann, H.; Sun, Z.; Palke, A.C. Color-Change SPESSARTINE Garnet: A First Report. *Gems Gemol.* **2019**, *55*, 254–257.
15. Kong, B.; Zou, J.F.; Shen, Y.P.; Luo, Y.Q. A primary study of alexandrite effect garnet from toliara, madagascar. *J. Guilin Inst. Technol.* **2000**, *A1*, 27–30.
16. Pei, J.-C.; Huang, W.-Z.; Zhang, Q.; Zhai, S.-H. Chemical Constituents and Spectra Characterization of Demantoid from Russia. *Spectrosc. Spectr. Anal.* **2019**, *39*, 3849–3854.
17. Reed, S.J.B. Recent Advances in Electron-Microprobe Analysis. *Inst. Phys. Conf. Ser.* **1992**, *130*, 67–74.
18. Wang, F.; Ge, G.; Ning, S.; Nie, L.; Zhong, G.; White, N.C. A new approach to LA-ICP-MS mapping and application in geology. *Acta Petrol. Sin.* **2017**, *33*, 3422–3436.
19. Shen, J.; Qin, L.; Fang, Z.; Zhang, Y.; Liu, J.; Liu, W.; Wang, F.; Xiao, Y.; Yu, H.; Wei, S. High-temperature inter-mineral Cr isotope fractionation: A comparison of ionic model predictions and experimental investigations of mantle xenoliths from the North China Craton. *Earth Planet. Sci. Lett.* **2018**, *499*, 278–290. [[CrossRef](#)]
20. Liu, Y.; Hu, Z.; Gao, S.; Guenther, D.; Xu, J.; Gao, C.; Chen, H. In situ analysis of major and trace elements of anhydrous minerals by LA-ICP-MS without applying an internal standard. *Chem. Geol.* **2008**, *257*, 34–43. [[CrossRef](#)]
21. Wang, J.-R.; Wang, Y.-M.; Zhang, D.-Q.; Liu, Z.-D.; Wang, C.-W.; Yin, K.; Gao, X.-W.; Xu, Y. FTIR Investigation of garnet: Indication for Specific Species and Coloration: A Case Study of a Yellow Garnet. *J. Gems Gemmol.* **2020**, *22*, 20–25.
22. Amthauer, G.; Rossman, G.R. The hydrous component in andradite garnet. *Am. Miner.* **1998**, *83*, 835–840. [[CrossRef](#)]
23. Yang, Y.; Xia, Q.; Feng, M. In situ FTIR investigations on nominally anhydrous minerals at varying temperatures. *Acta Petrol. Sin.* **2011**, *27*, 566–578.
24. Rossman, G.R.; Aines, R.D. The Hydrous Components in Garnets—Grossular-Hydrogrossular. *Am. Miner.* **1991**, *76*, 1153–1164.
25. Adamo, I.; Gatta, G.D.; Rotiroti, N.; Diella, V.; Pavese, A. Green andradite stones: Gemmological and mineralogical characterisation. *Eur. J. Mineral.* **2011**, *23*, 91–100. [[CrossRef](#)]
26. Geiger, C.A.; Rossman, G.R. IR spectroscopy and OH<sup>-</sup> in silicate garnet: The long quest to document the hydrogarnet substitution. *Am. Miner.* **2018**, *103*, 384–393. [[CrossRef](#)]

27. Geiger, C.A.; Stahl, A.; Rossman, G.R. Single-crystal IR- and UV/VIS-spectroscopic measurements on transition-metal-bearing pyrope: The incorporation of hydroxide in garnet. *Eur. J. Mineral.* **2000**, *12*, 259–271. [[CrossRef](#)]
28. Moore, R.K.; Bin, W.W. Electronic spectra of transition metal ions in silicate garnets. *Can. Mineral.* **1972**, *11*, 791–811.
29. Taran, M.N.; Dyar, M.D.; Matsyuk, S.S. Optical absorption study of natural garnets of almandine-skiagite composition showing intervalence  $\text{Fe}^{2+} + \text{Fe}^{3+} \rightarrow \text{Fe}^{3+} + \text{Fe}^{2+}$  charge-transfer transition. *Am. Miner.* **2007**, *92*, 753–760. [[CrossRef](#)]
30. Yang, P.; Guo, Y. New Insights into Coloration Mechanism in Violet-Red Pyrope-Almandine. *Crystals* **2022**, *12*, 379. [[CrossRef](#)]
31. Gübelin, E.; Schmetzer, K. Gemstones with alexandrite effect. *Gems Gemol.* **1982**, *18*, 197–203. [[CrossRef](#)]
32. Schifer, V.V. *Spectroscopy, Luminescence and Radiation Centers in Minerals*; Springer: New York, NY, USA; Berlin/Heidelberg, Germany, 1979.
33. Stubna, J.; Bacik, P.; Fridrichova, J.; Hanus, R.; Illasova, L.; Milovska, S.; Skoda, R.; Vaculovic, T.; Cernansky, S. Gem-Quality Green Cr-Bearing Andradite (var. Demantoid) from Dobsina, Slovakia. *Minerals* **2019**, *9*, 164. [[CrossRef](#)]
34. Sun, Z.-Y.; Palke, A.C.; Renfro, N.D.; Breitzmann, H.; Hand, D.; Muyal, J. Discovery of color-change chrome grossular garnets from Ethiopia. *Gems Gemol.* **2018**, *54*, 233–236.
35. Zwaan, J.C. Colour-Change Garnet from Tanga, Tanzania. *J. Gemmol.* **2020**, *37*, 133–134. [[CrossRef](#)]
36. Krambrock, K.; Guimaraes, F.S.; Pinheiro, M.V.B.; Paniago, R.; Righi, A.; Persiano, A.I.C.; Karfunkel, J.; Hoover, D.B. Purplish-red almandine garnets with alexandrite-like effect: Causes of colors and color-enhancing treatments. *Phys. Chem. Miner.* **2013**, *40*, 555–562. [[CrossRef](#)]
37. Makreski, P.; Runcevski, T.; Jovanovski, G. Minerals from Macedonia. XXVI. Characterization and spectra—Structure correlations for grossular and uvarovite. Raman study supported by IR spectroscopy. *J. Raman Spectrosc.* **2011**, *42*, 72–77. [[CrossRef](#)]
38. Giuliani, G.; Boiron, M.C.; Morlot, C.; Raoul, J.; Chatagnier, P.Y. Demantoid garnet with giant fluid inclusion. *Gems Gemol.* **2015**, *51*, 446–448.
39. Adamo, I.; Bocchio, R.; Diella, V.; Caucia, F. Demantoid from Balochistan, Pakistan: Gemmological and Mineralogical Characterization. *J. Gemmol.* **2015**, *34*, 428–433. [[CrossRef](#)]
40. Pezzotta, F.; Adamo, I.; Diella, V. Demantoid and Topazolite from Antetazambato, Northern Madagascar: Review and New Data. *Gems Gemol.* **2011**, *47*, 2–14. [[CrossRef](#)]
41. Ahadnejad, V.; Krzemnicki, M.S.; Hirt, A.M. Demantoid from Kerman Province, South-east Iran: A Mineralogical and Gemmological Overview. *J. Gemmol.* **2022**, *38*, 329–347. [[CrossRef](#)]
42. Buhn, B.; Okrusch, M.; Woermann, E.; Lehnert, K.; Hoernes, S. Metamorphic Evolution of Neoproterozoic Manganese Formations and Their Country Rocks at OTJOSONDU, NAMIBIA. *J. Petrol.* **1995**, *36*, 463–496. [[CrossRef](#)]
43. Bocchio, R.; Adamo, I.; Diella, V. The Profile of Trace Elements, Including the REE, in Gem-Quality Green Andradite from Classic Localities. *Can. Mineral.* **2010**, *48*, 1205–1216. [[CrossRef](#)]

**Disclaimer/Publisher’s Note:** The statements, opinions and data contained in all publications are solely those of the individual author(s) and contributor(s) and not of MDPI and/or the editor(s). MDPI and/or the editor(s) disclaim responsibility for any injury to people or property resulting from any ideas, methods, instructions or products referred to in the content.